Journal of Intelligent & Robotic Systems (2023) 109:59
https://doi.org/10.1007/s10846-023-01999-9

REGULAR PAPER

Towards Robust Physical Human Robot Interaction by an Adaptive Admittance Controller

Guanghui Liu[1] · Qiang Li[2] · Lijin Fang[1] · Hualiang Zhang[3]

Received: 2 March 2022 / Accepted: 11 October 2023 / Published online: 3 November 2023

Abstract
The regular admittance controller cannot be easily transferred to the physical human–robot interaction scenario because of the dynamic stiffness of the human arm. The dynamic interaction of humans can cause high frequency and unsafe oscillation of the robot arm. Based on the adaptive control scheme, this paper presents an online sensory-based analytical approach to recognize and quantify the “stability index" named as a robust haptic observer. The observer performs the Fast Fourier Transform on the interaction force signal within a sliding window and quickly detects system oscillation through a simple mathematical transformation. Compared with the existing methods, it can calculate a normalized system stability index more accurately and faster. This quantified index is employed in a linearized adaptive law to tune the parameters of the admittance controller. Experimental validation of the proposed strategy is performed and compared with state-of-the-art work in a task of human-guided drawing. The results show that our proposed approach can effectively detect oscillation, and the drawing time is shortened by 15% with the same tracking accuracy. In addition, the energy consumption is 44.4% less on average.

Keywords Adaptive admittance control · Stability observer · Frequency analysis · Compliance control

1 Introduction

Physical human–robot interaction (pHRI) is an important feature of the new generation of collaborative robots. In recent years, a growing interest for pHRI, that a robot implements the assisted manipulation tasks, can be observed in many industrial applications. One of representative applications is to teach robots new skills by human-guided robot movement [1], such as the scenario in Fig. 1. In order that the skills can be demonstrated easily, the robot needs to work in the "gravity compensation" mode, in which human can guide the robot arm with less effort. To this end, different sensory-based approaches–force/torque sensor [2], tactile sensor [3] joint torque sensing [4, 5] and electric current [6, 7], have been studied to design the robot’s admittance controller.

Traditional admittance controllers in robotic manipulation domain cannot be directly transferred to the human-guided tasks because they are mainly designed for a static payload [8] or contacts environment with less variance [9, 10]. The main challenge that human-guided tasks brought to robotic control is the unknown and dynamic interact force which depends on the human's habit and given tasks. To this end, the controller should be online, real-time and also adaptive. The proper computation of the controller parameters is crucial for successful and robust human-guided tasks. Such parameters not only affect the stability of the human–robot system, but also affect the performance of the guiding, e.g. whether the robot can follow the operator’s movement with less human’s effort [11]. Neuroscience and neurocontrol studies [12–14] in human robot interaction tasks showed that, human had an adaptive capability with external disturbance by tuning their arms stiffness, and research in control engineering domain also was reported that the robot's stability strongly depended on admittance parameters in human robot interaction tasks [15–18]. Given the improper admittance parameters, the robot is apt to be unstable. As a

Guanghui Liu and Qiang Li contributed equally to this work.

✉ Lijin Fang
ljfang@mail.neu.edu.cn

[1] Faculty of Robot Science and Engineering, Northeastern University, Shenyang, China

[2] Neuroinformatics Group & CITEC, Bielefeld University, Bielefeld, Germany

[3] Shenyang Institute of Automation, Chinese Academy of Sciences, Shenyang, China

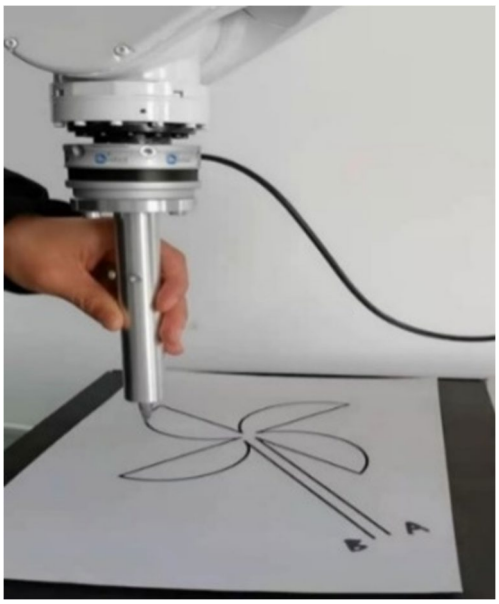

Fig. 1 Human guiding a robot for drawing a complex pattern

consequence, the robot behavior is deviated from the desired one and finally the robot oscillated with high amplitude and frequency, namely an unsafe interaction state. So, it is necessary to study how to detect the arising of oscillations and then generate adaptive control command to drive robot back to the stable and safe state.

Different approaches were proposed to improve the instability of the pHRI system. Tsumugiwa et al. [19] proposed to tune the virtual damping coefficient in proportion to the estimated stiffness of the human arm. Wang et al. [20] estimated the human arm's stiffness with recursive experiments, defined the Lyapunov function and the stability frontiers for the closed-loop system [21]. Besides, an estimation of human arm impedance or intention was used for the variable impedance controller [22–24]. The analytical model of the robot and the human arm was calculated and the admittance parameters were adjusted relative to the stiffness of the human arm. However, the hysteresis of the output response of the robot's position control loop is not considered. Moreover, this requires the analytic model in advance, and the estimation is not accurate because of the simplification of the model.

Another research line is based on the frequency analysis of online measured force/position. In [25], authors proposed a haptic stability observer (HSO) algorithm. The frequency analysis of the interaction force signal was done and stability index was defined to detect the interaction oscillation. Consequently, the admittance parameters (e.g. mass inertia and virtual damping) were tuned proportionally. The main problem of HSO is that the stability index cannot clearly distinguish the different frequencies oscillation and the big detection threshold limits the value range of the stability index. Dimeaset al. [26] proposed a haptic stability observer with scaling factor (HSOSF). Although this approach took online recursive strategy to improve the detection accuracy of stability index in different frequencies, it caused the delay of observation and the computed stability index was not normalized. Finally, the main limitations of the current variable admittance control methods are briefly concluded in Table 1.

Table 1 Variable admittance control methods for physical human–robot interaction

Method	Limitations
Human intention estimation	- additional setup needed - complicated training process
Human arm's stiffness estimation	- no accurate model - estimation delay
Frequency analysis (HSO/HSOSF)	- calculation delay - no normalized index

The whole paper is organized in the following way. Section 2 introduces the admittance control framework. In Section 3, Robust Haptic Stability Observer (RHSO) is proposed and followed by the admittance parameters adaptive law in Section 4. The experiment evaluations for the proposed observer and adaptive law are shown in Section 5. Finally, Section 6 gives the conclusion and future work.

2 Adaptive Admittance control framework for pHRI

The admittance control scheme is widely used for compliant motion of the position-controlled robot. The controller gets the input of externally applied forces/torques and outputs the position of the robot by establishing a second order system relationship among position, velocity, acceleration and force. In most common tasks, contact only happens in the robot's end-effector, and the relationship is formalized as:

$$M_d(\ddot{x}_d - \ddot{x}_m) + B_d(\dot{x}_d - \dot{x}_m) + K_d(x_d - x_m) = F_{ext} \tag{1}$$

where $\dot{x}_d$ and $\dot{x}_m$ are the desired and measured velocity of the end-effector, respectively. The controller gains M_d, B_d and K_d are 6-by-6 diagonal matrices, representing the virtual inertia, the virtual damping and the virtual stiffness, respectively. Since the restoring forces are not desirable during pHRI in free-space [2], the virtual stiffness is omitted in the study of this paper.

$$M_d(\ddot{x}_d - \ddot{x}_m) + B_d(\dot{x}_d - \dot{x}_m) = F_{ext} \tag{2}$$

By transforming and discretizing Eq. 2:

$$\ddot{x}_d(kT) = \ddot{x}_m(kT) + \frac{1}{M_d}\left(F_{ext}(kT) - B_d\left[\dot{x}_d[(k-1)T] - \dot{x}_m(kT)\right]\right) \tag{3}$$

where $\dot{x}_m = J\dot{q}_m, \ddot{x}_m = \dot{J}\dot{q}_m + J\ddot{q}_m \bullet \dot{q}_m$ is the velocity of joint, and it is computed as differentiation of the joint position. Similarly, $\ddot{q}_m$ can be calculated as the differentiation of $\dot{q}_m$ .J is the Jacobian matrix of the robot. Note that, $\dot{x}_d(kT)$ has been replaced by $\dot{x}_d[(k-1)T]$, and $\dot{x}_d(0)$=0.

Given the Eq. 3, the whole admittance scheme including the robot is illustrated as Fig. 2. It is composed of four blocks—robot model block, human–robot interaction block, admittance control block and adaptive parameters block. The robot's dynamical model can be obtained experimentally and the transfer function $G_0(s)$ between measurement x_m and command x_d is estimated [7]. Inspired by [16], this paper explicitly models the human–robot interaction as a first-order system, including a human operation delay element $1/(T_H + 1)$ and an element K_E for representing the stiffness of the environment (human arm). Previous studies showed that such simplified model is enough to the muscle characteristics of human arm [16].

From Eq. 2, the admittance controller with the form of the transfer function can be rewritten as Eq. 4.

$$Y(s) = \frac{x_d(s)}{F_{ext}(s)} = \frac{1}{M_d s^2 + B_d s} \tag{4}$$

The closed-loop transfer function of pHRI system considering contact force as input and measured pose of the robot end-effector as output is obtained as following:

$$\frac{x_m(s)}{F_{ext}(s)} = \frac{Y(s)G_0(s)}{1 + K_E H(s)Y(s)G_0(s)} \tag{5}$$

where K_E is the stiffness of human arm, $H(s)$ is the time delay element with regard to the reaction of a human operator.

In order to improve the robustness of pHRI, the parameters M_d, B_d are adaptively tuned by the online estimated stability index and empirical adaptive law, which is the main functionality of the adaptive parameters block. It is composed of a Robust Haptic Stability Observer (RHSO) and an adaptive law algorithm. Using the stability index calculated by RHSO, the adaptive law will tune the controller's admittance parameters and guide pHRI system back to the stable state.

3 Robust Haptic Stability Observer

3.1 Haptic Stability Observer (HSO)

HSO is used for detecting and quantifying the stability. With observer, the stability is described not by the computed features (energy and velocity) but by direct measurements (force and position). Based on HSO, a controller can be designed to suppress instability.

By monitoring the external force applied by the operator, the magnitude $P_f(\omega)$ of the frequency components ω can be calculated using FFT. A rough indication of instability is computed as by the ratio of the sum of magnitudes P_f of the high frequency components to the sum of magnitudes of all frequencies:

$$I_p[kT] = \frac{\sum_{\omega=\omega_c}^{\omega_s/2} P_f(\omega)}{\sum_{\omega=\omega_0}^{\omega_s/2} P_f(\omega)} \tag{6}$$

$$\begin{cases} I_p < \varepsilon, & \text{stable} \\ I_p \geq \varepsilon, & \text{unstable} \end{cases} \tag{7}$$

where I_p is the index of system stabiliby, ω_0 is the lowest frequency of the FFT, $\omega_s/2$ is determined from the Nyquist-Shannon sampling theorem and $P_f(\omega)$ is the amplitude of the ω frequency component. The frequency ω_c depends on the robot dynamics and is determined experimentally. It represents the crossover frequency used to distinguish between frequency components of stable and unstable motion ε in Eq. 7 is the threshold of the stability.

The frequency components $P_f(\omega)$ are computed by implementing FFT on a window with the N latest measurements of the force signal. When the sampling period T is selected, the window period of FFT is $T_w = NT$, and the frequency resolution is $\Delta f = 1/T_w$.

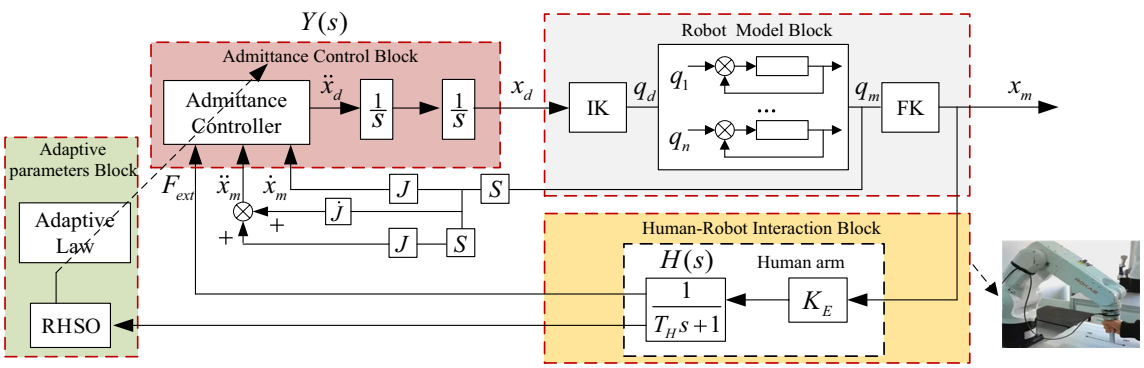

Fig. 2 The scheme of adaptive admittance control for pHRI

3.2 Robust Haptic Stability Observer(RHSO)

The main problem of HSO is that the stability index cannot clearly detect the different frequencies oscillation. In this paper, the robust haptic stability observer is proposed.

$$I_{sp} = \begin{cases} \frac{I_p}{1+\varepsilon}, (I_p < \varepsilon) \\ \frac{I_p - \varepsilon}{1+\varepsilon} + \frac{\varepsilon}{1+\varepsilon}, (I_p \geq \varepsilon) \end{cases} \tag{8}$$

$$\begin{cases} I_{sp} < \lambda = \frac{\varepsilon}{1+\varepsilon}, & \text{stable} \\ I_{sp} \geq \lambda = \frac{\varepsilon}{1+\varepsilon}, & \text{unstable} \end{cases} \tag{9}$$

This paper redefine the stability index, as Eq. 8 and Eq. 9. I_{sp} and λ are system stability index and threshold of RHSO, respectively. According to Eq. 6, the value of stability index in HSO is always high even without contact because of the noise output from force sensors. For example, in [22] authors had to use higher threshold to detect the oscillation. To this end, the stability index calculated by HSO is usually almost the same even the oscillation degrees are apparently different. This means that the stability index in HSO cannot effectively describe the degree of system oscillation. Unlike HSO, our proposed method linearly reduces the stability index, so that the threshold of stability can be set smaller. When the system is unstable, RHSO effectively enlarges the range of stability index from $[\varepsilon, 1]$ to $[\varepsilon/(1+\varepsilon), 1]$. Therefore, RHSO can sensitively provides the quantified stability for different oscillation degrees, as shown in Fig. 3.

Secondly, it can be found that the time delay for ossillation detection in [23] was caused by the long sample window. To this end, in RHSO, a sliding data window is applied. A fixed size FFT window is defined, take FIFO strategy and use the historical and a small part updated data at every sampling period. It not only guarantees the resolution of the oscillation detection but also improves the real-time performance of detection.

The whole algorithm is described in Algorithm 1. It represents the observer employed in one dimension direction, which can be easily extended and used in all six dimensions.

$f[n]$ is the temporal queue of force/torque signal used by FFT, and N is the length of the queue. u is the number of $f[n]$ updated for FFT each time. ε, λ are the thresholds of HSO and RHSO stability, respectively.

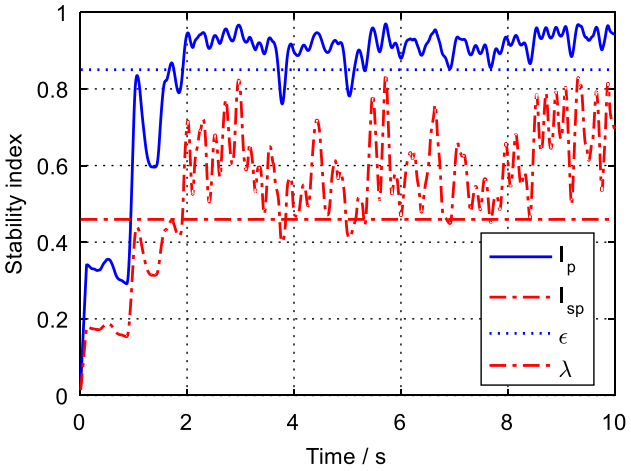

Fig. 3 The stability index of RHSO is calculated by Eq. 8. The RHSO effectively reduces the threshold of the stability index, so that it can distinguish the oscillation degree obviously

4 Admittance Parameters Adaptive Law Using RHSO

4.1 The Adaptive Law of Admittance Parameters

The stiffness of human arm is the main factor leading to the instability of the robot. In the admittance controller, increasing the damping coefficient B_d can increase the stability margin of the robot. However, the accompanied cost is the more efforts are needed from human in order to guide the robot. Experimental study [19] showed that, when the robot is in unstable state, given the constant M_d and the increased damping, the oscillation amplitude is decreased. However, the oscillation frequency will not be decreased by only increasing the damping coefficient. Increasing M_d and keeping B_d as a constant value, the oscillation frequency is decreased, but the amplitude is unchanged. This stimulates authors to design an adaptative law to simultaneously tune the admittance controller parameters, in order that the whole pHRI can keep a balanced amplitude frequency characteristics. The adaptive law is formalized as:

$$\begin{aligned} M_d[kT] &= M_d^{\min} + M_r I_{sp}[kT] \\ B_d[kT] &= B_d^{\min} + B_r I_{sp}[kT] \end{aligned} \tag{10}$$

where I_{sp} is the normalized stability index (Algorithm 1) of the robot.M_d^{min}, B_d^{min} are the minimum values for the virtual inertia and damping respectively, which are emperically designed for stable and less-effort guiding motion. In practice, they are the lowest permissible values for stable operation of the robot without being affected by the noise of the force sensor. M_r, B_r are the reference value to make the robot stable. In practice they are designed as the virtual inertial and virtual damping while the stiffness of the human is maximum and the robot is in critical stable. It needs to be mentioned, in practice $M_r \gg M_d^{min}$, $B_r \gg B_d^{min}$.

In order to discuss the relationship between parameters and system stability, root locus and lookup table approach is used to design feasible parameters for Eq. 10. Given the transfer function (Eq. 5) which is parameterized by M_d, B_d and K_E, it firstly computes and draws root locus curve of one of parameters considering other two parameters are fixed. From the computed root locus, the parameter values while the robot is

Algorithm 1 Robust Haptic Stability Observer (RHSO)

Data: $f[n], u, \omega_0, \omega_c, \omega_s, \varepsilon, \lambda = \varepsilon/(1+\varepsilon)$

Initialize $f[0], f[1], \cdots, f[N-1] = F_{ext}(0)$

for $i = 0$ **to** ∞ **do**

update one data of queue $f[n]$ each sampling period

if $i \,\%\, u == 0$ **then**

compute frequency components $P_f(\omega)$ of $f[n]$ by FFT

compute Haptic Stability Observer Index

$$I_p = \frac{\sum_{\omega=\omega_c}^{\omega_s/2} P_f(\omega)}{\sum_{\omega=\omega_0}^{\omega_s/2} P_f(\omega)}$$

compute RHSO stability Index

if $I_p < \varepsilon$ **then**

$$I_{sp} = \frac{I_p}{1+\varepsilon}$$

else if $I_p \geq \varepsilon$ **then**

$$I_{sp} = \frac{\frac{I_p - \varepsilon}{1-\varepsilon} + \varepsilon}{1+\varepsilon}$$

end

if $I_{sp} < \lambda$ **then**

$I_{sp} = 0$, system is stable

else if $I_{sp} \geq \lambda$ **then**

$I_{sp} = I_{sp}$, system is unstable

end

end

end

in critical stable can be obtained. Using this strategy, sampling M_d and K_E in a physically rational range, B_d–a damping value mapping table can be formed with the given virtual inertia and human arm stiffness. In order that this analysis approach can be easily understood for readers, the analysis using one industrial robot as an example is done in Section 5.1. The emperical parameters required for Eq. 10 are selected in the experiments at Section 5.2. and Section 5.3.

4.2 Index of Human Effort in the Guiding Task

In order to compare the human effort required for the guiding task with different admittance controllers, the index of the effort as the total energy transferred from the human to the robot is defined. It is calculated by the integral of the force $|f_h|$ over the total traveled distance x_f:

$$P = \int_0^{x_f} |f_h| dx \tag{11}$$

5 Experimental Evaluation

Experimental evaluations were performed using a ROKAE XB7 6-DOF robot equipped with a 6 axis F/T sensor (OnRobot HEX-E v2) mounted on the end-effector [7].The robot has control interface for joint position with the sampling and control frequency up to 1 kHz. The robot's weight and maximum payloads are 47 kg and 7 kg, repectively.

5.1 Stability Analysis And Admittance Parameters Table

Robot's stability depends on the simultaneously tuning of parameters in admittance controller block. In this part, using ROKAE XB6 as an example, the relation among parameters employing the root locus of pHRI model (Eq. 4, Eq. 5) is analyzed. The transfer function G_0(s) of the robot is given as follows:

$$G_0(s) = \frac{1.45e-6s^3 - 0.75s^2 + 3.92e5s + 5.48e7}{s^4 + 190.9s^3 + 2.73e4s^2 + 1.72e6s + 5.55e7} \quad (12)$$

The equivalent robot parameters in Eq. 5 are calculated for the configuration with $M_d = 0.25kg, B_d = 0.5\text{Ns/m}, T_H = 0.001\text{s}$, $K_E = 10\text{N/m}$. The root locus module provided by MATLAB toolbox was used. With the given model parameters in Eq. 5, the root locus of K_E, B_d are drawn in Fig. 4(a) and (b), respectively. It is illustrated in Fig. 4(a), with the increasing of the human arm stiffness, the root locus will pass through the Real Axis, and the system will be unstable. The K_E is selected when the root locus is passing through the Real axis as the human arm's stiffness in the critical stable. From the Fig. 4(b), it is clearly showned that increasing the damping coefficient B_d is an effective way to make the system more stable. The B_d is selected when the root locus is passing through the Real axis as the virtual damping in the critical stable.

Figure 5 can more intuitively show the relation among stiffness, damping and inertia for the stability. Increasing K_E and keeping M_d and B_d as constant values, the oscillation amplitude is decreased, but the oscillation frequency is increased. Given the constant M_d, K_E and the increased damping, the oscillation amplitude is decreased. However, the oscillation frequency will not be decreased. Increasing M_d and keeping B_d and K_E as constant values, the oscillation frequency is decreased, but the amplitude is increased. Keeping constant ratio— M_d/B_d and increasing both parameters are effective admittance adaption to reduce the magnitude and frequency of oscillation.

Three M_d values 0.01 kg, 0.5 kg and 1 kg, and seven K_E from 0.25N/m to 2000N/m are sampled. Using the approach proposed in Sec IV.A. The different B_d of system critical stable state are obtained. As shown in Fig. 6, there are three different critical stability lines which is relevant to three virtual inertias. The whole stiffness and damping–plane is divided into stable region and unstable region by each critical stability line. It is noticed that the increasing of the virtual inertia M_d will make the system stable region smaller. In addition, as long as the human arm stiffness is less than the critically stable stiffness, the system will be stable. With transfer function (Eq. 12), more M_d and K_E are sampled to obtain a virtual damping parameters table while the robot is in the critical stable state. It is shown in Table 2.

5.2 Evaluation of Stability Index Computed by HSO, HSOSF and RHSO

In this experiment, RHSO approach is compared with HSO and HSOSF in computing stability index and detecting the oscillation in a point to point task. As shown in Fig. 7, a human is asked to guide the robot moving 160 mm -repeatly

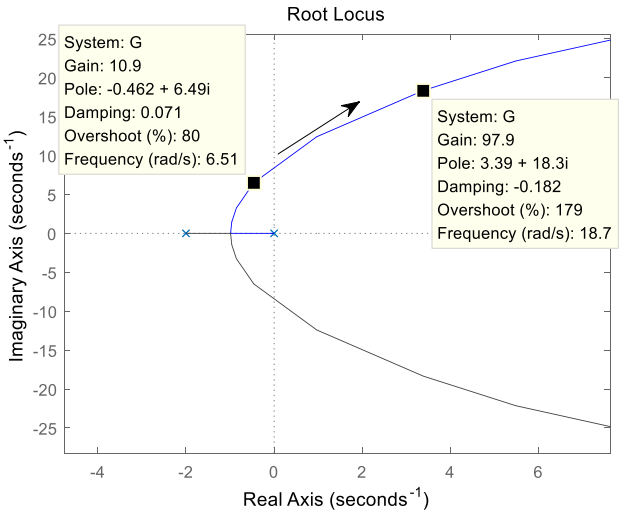

(a) Root locus of the system considering human arm stiffness as variable and virtual inertia and virtual damping are fixed.

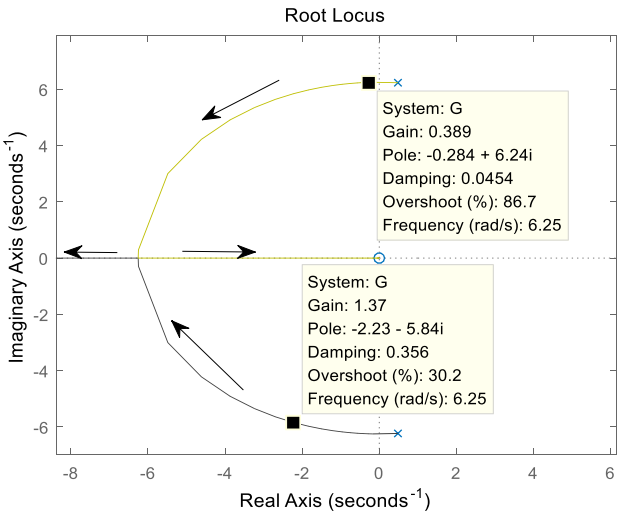

(b) Root locus of the system considering virtual damping as variable and virtual inertia and human arm stiffness are fixed.

Fig. 4 System stability analysis considering three parameters: virtual inertia, virtual damping and human arm stiffness

from point A to point B and back to point A as fast as possible along the X-axis. The admittance parameters along X-axis are set as $M_d^x = 0.003kg, B_d^x = 0.006Ns/m$. These parameters were used because it is known that the robot is at the boundary of the stable region with such fixed parameters according to parameters Table 2. In other directions, parameters are set as $M_d^{\{y,z,\alpha,\beta,\gamma\}} = 1kg$, $B_d^{\{y,z,\alpha,\beta,\gamma\}} = 50Ns/m$. The experiments show that human can successfully guide robot moving by lightly pinching the handle. With the increasing stiffness of human arm, e.g. with power grasping, the guidance motion become unstable. The detailed guiding procedure is illustrated with accompanied video and explained as following.

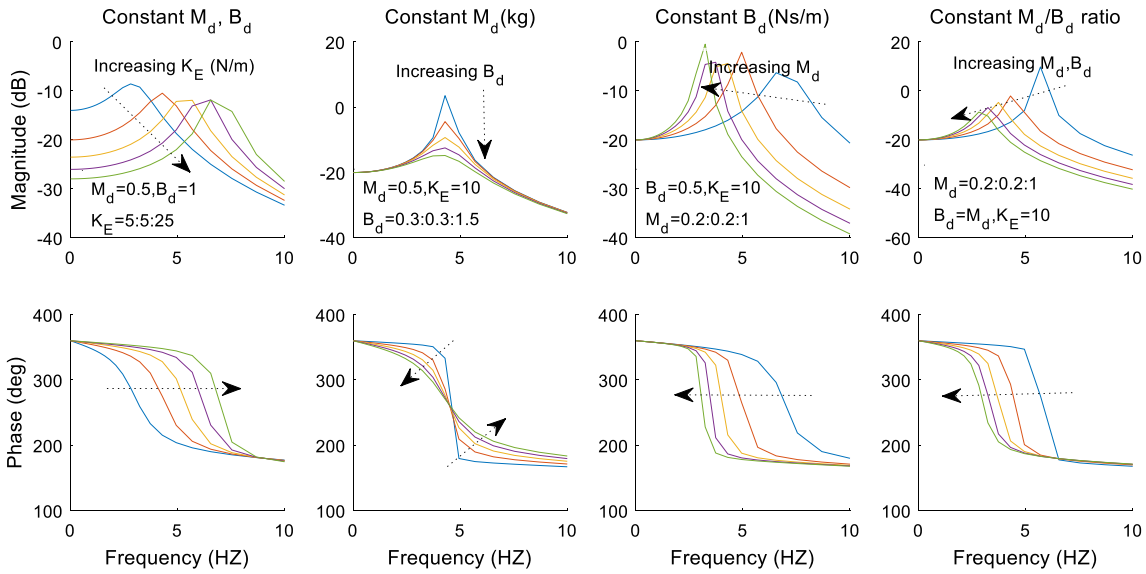

Fig. 5 Frequency response diagrams for different types of admittance adaptation

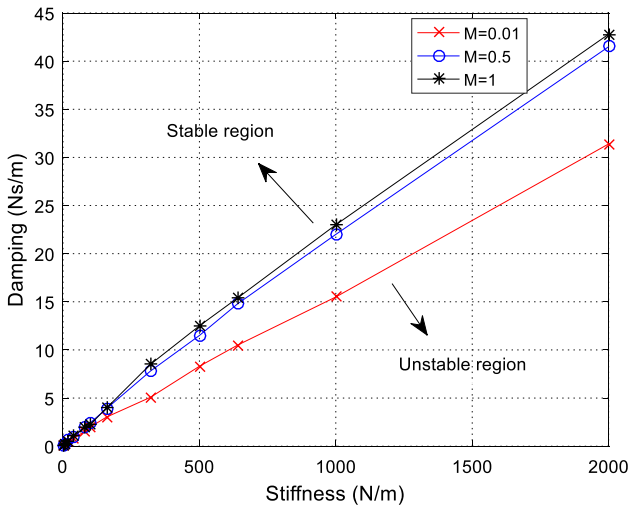

Fig. 6 System stability region division

In the initialized stage S0, there is no external contact and the robot keeps stationary. At the first stage S1, the human pinches the handle with two fingers and guides it from point A to point B and back to point A repeatly. The motion is required as fast as it can. At second stage S2, the human grasps the handle with moderate stiffness and does the guiding motion. At the third stage S3, the human is asked to grasp the handle as tightly as he can and move it like stage 2. Finally at the fourth stage S4, the human pinches the handle again and guides the robot motion. Experiment result shows that robot starts to oscillate at S2 and S3 stages with different frequencies and amplitudes. The measured external force and stages are shown in Fig. 8.

FFT is used to analyze the measured external force, and the frequency distribution is shown in Fig. 9. In the figure, the frequency of human guiding motion is lower than 2 Hz. The two unstable oscillations with frequency higher than 2 Hz are correspond to the S2 and S3 stages. The stability index employing HSO, HSOSF, RHSO are computed, respectively. Parameters required in the algorithms are set as $\omega_0 = 0$, $\omega_c = 2HZ$, $\omega_s = 20HZ$. Window length $n = 1024$. Algorithm in HSOSF [22], three more parameters are required $\gamma = 0.99$, $f_{max} = 15N$, $p = 5$. The comparing result is shown in Fig. 10.

Table 2 Virtual damping value while pHRI is in critical stable given the virtual inertia and human arm stiffness (one dimention)

K_E(N/m)	M_d(kg)					
	0.0025	0.01	0.25	0.5	0.75	1
0.25	0.0051	0.0098	0.0261	0.0365	0.0444	0.0510
10	0.191	0.232	0.332	0.428	0.521	0.609
100	1.620	1.990	2.290	2.430	2.440	2.250
500	7.48	8.30	11.00	11.50	12.80	12.50
1000	16.10	15.50	19.01	22.00	23.51	23.00
2000	30.52	31.40	38.11	41.50	41.98	43.12

Fig. 7 Human guiding for a robot's linear motion

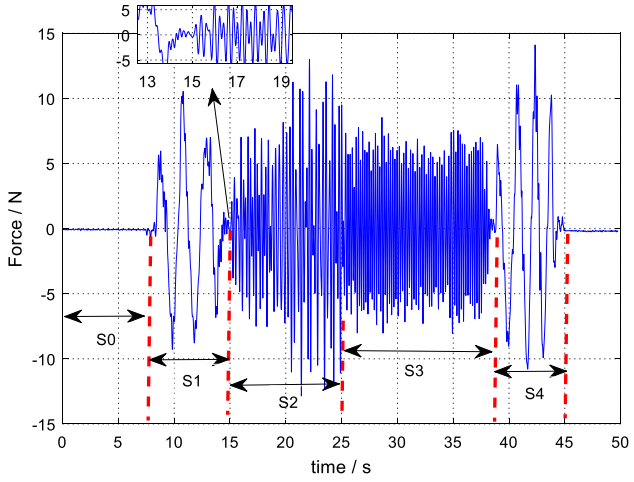

Fig. 8 Contact force profile in five stages in the task of the human guiding the robot for linear motion. the top-left small figure is the enlarged view of contact force from 13–19 s. S0: no contact, S1: guiding with pinching the handle and low stiffness, S2: guiding with power grasping but moderate stiffness, S3: guiding with power grasping but high stiffness, S4: guiding with pinching the handle and low stiffness. At the S1 and S4 stages, human can guide the robot stably. The robot is unstable and oscillation frequency at stage S3 is higher than at stage S2 because of the higher human arm stiffness. This is consistent with the FFT analysis in Fig. 9

As shown in Fig. 10, at stage S0, there is no external contact, and the stability index computed by HSO is a positive value, which is mainly caused by the force/sensor noise. This stage can be classified as stable if the threshold is set higher. The stability index from HSOSF is close to 0, which is a a good sign to show the robot is in the stable stage. The stability index from our approach has a middle-level output which has a better margin compared with the HSO approach. In stage S1, the robot is stably guided by a human. Our approach has the best margin for designing stability thresholds. At stage S2, the robot is in the unstable stage. The computed stability index from HSOSF has a delay, and the threshold required for correctly classifying the state is larger than the other two approaches, Although the stability index calculated by RHSO also has positive values at the S0 and S1 stages, it is less than the values computed from HSO. At the S2 and S3 stages, compared with HSO, the RHSO not only detects the instability motion but also effectively distinguishes the difference between the stages from the oscillation frequency. From the top-left small figure in Fig. 8, the robot starts to oscillate at around 15.0 s. It is detected by HSO at around 15.5 s. In contrast, the RHSO method detects system oscillations in a more timely manner at around 15.0 s.

5.3 Evaluation for Guiding Efficiency, Accuracy and Human's Effort with Proposed Adaptive Controller

This experiment is used to verify the RHSO and adaptive admittance controller in a challenging tracking task. The task is illustrated in Fig. 1, the human is required to guide the robot following a windmill shaped pattern on the X–Y plane as accurately and quickly as possible. The experiments are done by five person and everyone does 5 trials before the recorded experiments are done. One of results is show in Fig. 11.

In the experiment, the robot is compliance in X and Y dimension, while in other dimensions, virtual inertias and virtual dampings are set to large values: $M_d^{\{z,\alpha,\beta,\gamma\}} = 1kg$, $B_d^{\{z,\alpha,\beta,\gamma\}} = 50Ns/m$. In X, Y directions, three groups parameters are used: Min parameters, Max parameters and adaptive parameters proposed in Eq. 10. The Min parameters are set as $M_d^x = 0.0025kg$, $M_d^y = 0.0025k$, $B_d^x = 0.006Ns/m$, $B_d^y = 0.006Ns/m$. Damping value is slightly larger than the critical damping parameters while $K_E = 0.25N/m, M_d = 0.0025kg$, in Table 2. According to Fig. 5, the robot is staying in stable region with slight margin when the human guides it with low stiffness. When the stiffness of the human arm is increased, the system will be unstable. The Max parameters are $M_d^x = M_d^y = 0.5kg$, $B_d^x = B_d^y = 23.0Ns/m$. As in Table 2, as long as the human arm stiffness is less than $1000N/m$ (Normally, the muscle stiffness is less than this value [27]), the system will be stable with these parameters. The adaptive parameters are defined as $M_d^x = M_d^y = 0.0025 + M_r I_{sp}$, $B_d^x = B_d^y = 0.006 + B_r I_{sp}$. In this experiment, $M_r = 0.5kg, B_r = 23.0Ns/m$ are set because $M_r \gg M_d^{min}$, $B_r \gg B_d^{min}$.

In order to compare the tracking accuracy with different approaches, the index is defined as follows:

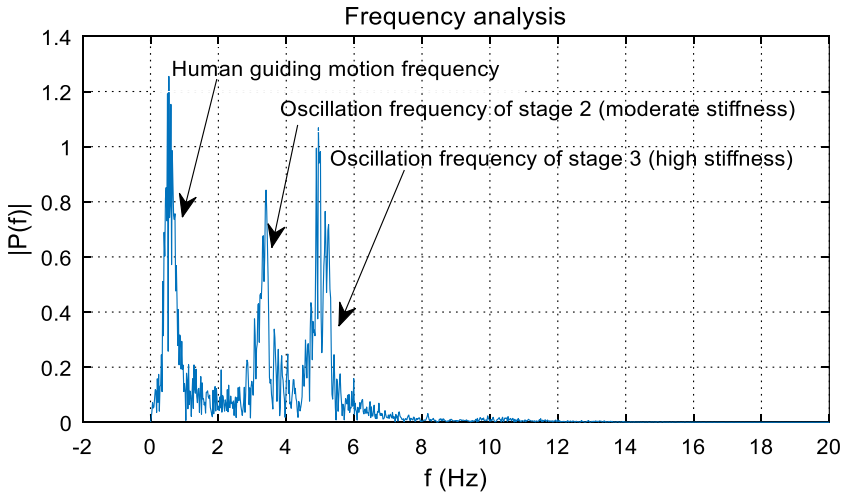

Fig. 9 Frequency distribution of the force signal

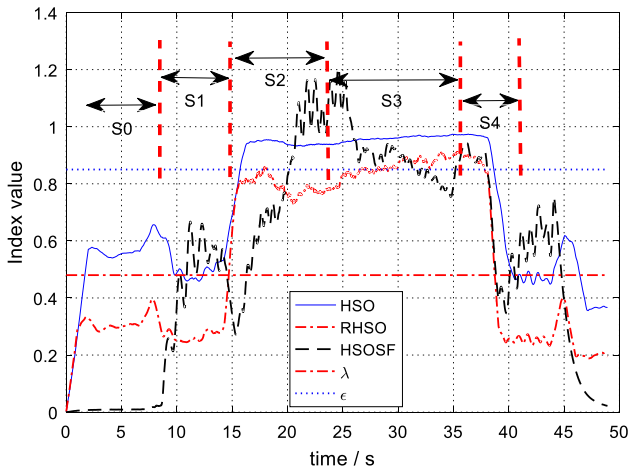

Fig. 10 Stability index computation from the measured force in Fig. 8 using three different observers. The robot is oscillating at stage 2 and 3 with different frequencies. Compared with HSO, RHSO stability index reflects this obviously and this is prerequisite that admittance parameters in controller can be tuned according to the stability index. It is also can be seen that the RHSO method detects the oscillations in a more timely manner than HSOSF

$$Var = \sum_{i=1}^{n} \frac{\|T_i(x,y) - R_i(x,y)\|}{\|R_i(x,y)\|} \tag{13}$$

where $T_i(x,y)$ is the dragging trajectory at the *ith* sampling-period, $R_i(x,y)$ is of the reference trajectory, and n is the number of robot trajectory points.

Tracking curve with "Max parameters" controller is more smooth. The downside is that the guiding task needs more human energy and the operator reported that he felt the robot was more "heavy" to guide. The "Adaptive Parameters" controller is an optimized method to minimize the energy consumption of the arm without reducing the tracking accuracy. One thing that needs to be mentioned is that

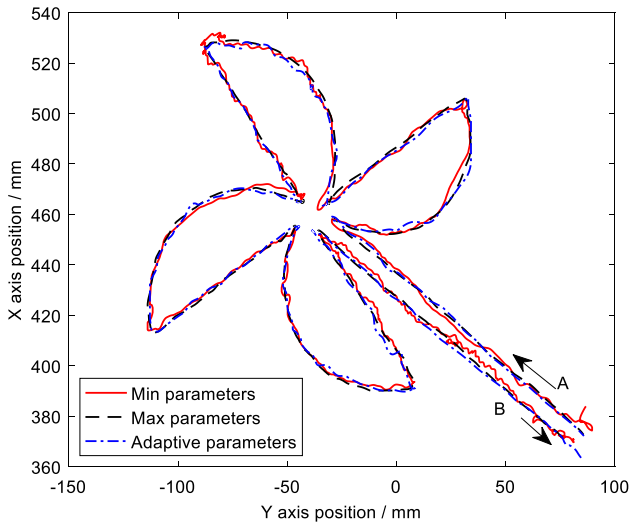

Fig. 11 Tracking results with different controllers

"Min parameters" controller only works when the human arm stiffness is low.

All operators are visualized, named A,B,C,D,E, drawing efficiency and accuracy in Fig. 12, which includes cost time, energy consumption and tracking variances. With the “Min parameters” controller, it costs the shortest time, but tracking accuracy is worse due to the robot is too “soft and sensitive”. Therefore, compared with the adaptive parameters controller, the "Min parameters" controller has more overshooting trajectories and more energy consumpation. With the “Max parameters” controller, it costs the longest time and highest energy, but tracking accuracy is best. Using the adaptive parameters, the costed time is longer than the time with “Min parameters” controller, but the stability is improved obviously. Besides, with the proposed method, human consumes the least energy. Even comparing with “Min parameters” controller, the energy consumption is 44.4% less averagely.

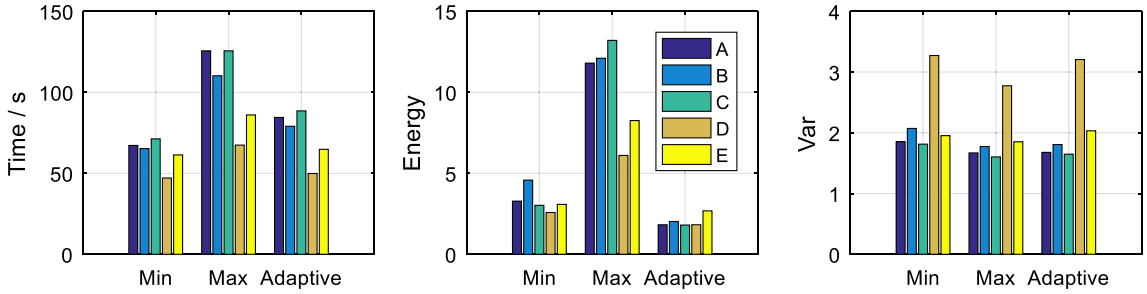

Fig. 12 Experiment results of Five operators, including consume time, energy consumption and position tracking variances

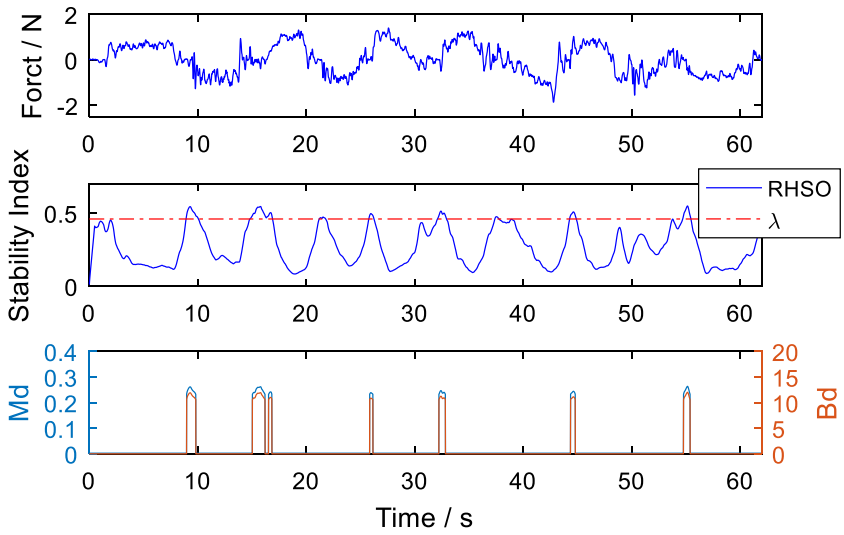

Fig. 13 Parameters of the adaptive method are depicted, including force signal, RHSO stability index, M_d and B_d of admittance controller. If the stability index is higher than the threshold, the adaptive admittance controller starts to work. The tuned parameters are bounded and smooth

Given the adaptive controller, the measured force, computed stability index and variable inertial mass and damping are visualized in Fig. 13. The experiment is illustrated in the accompanied video. It can be seen (1) there is no strong force oscillation. Only weak oscillation is found when the computed stability index is higher than the threshold. The adaptive controller quickly works and restrains the oscillation caused by the increased stiffness. (2) the stability index is smooth and continuous. There are several places, the stability index is higher than the threshold. The inertia mass and virtual damping are fine tuned in these places.

6 Conclusion

In this paper, an adaptive admittance controller for pHRI task is proposed. In the control framework, the measured force feedback and FFT approach are emploied to detect the robot's oscillations with a robust haptic stability observer. Our proposed method has advantage in many aspects comparing with state of the art approaches. e.g. less sensitive to non-contact sensing noise, no detection delay of the oscillation.

Given the admittance control scheme, an adaptive law exploiting the output of the observer is proposed to tune the admittance parameters of controller and restore the robot back to stable state once the interaction is unsafe. This paper demonstrates the functionality of the proposed adaptive controller with a human-guided drawing task. With the controller human can guide the robot with minimum effort and achieve better tracking accuracy and efficiency comparing with the fixed admittance parameters controller. The proposed adaptive law is a practical and empirical solution and uses classical root locus approach to design the controller parameters. Although a rigorous mathematical proof for the stability of the system is not provided, the linearized controller parameters calculated by lookup table can ensure the convergence of the system in the reasonable scope of human arm stiffness, virtual inertial and virtual damping from the opinion of classical control theory. Except this potential work in future, the authors also will study how the approach can be extended to other manipulation applications, e.g. cutting, sawing, peg-in-hole etc.

Authors' Contributions *Guanghui Liu*—Conceptulization, Methdology, Software, Data curation, Writing-original draft. *Qiang Li*—Software, Data curation, Validation, Writing—review & editing. *Lijin*

Fang—Supervision, Writing—review & editing. *Hualiang Zhang*—Supervision, Writing—review & editing.

Funding This research was supported by the China Scholarship Council under Grant (202106080049), and in part by "DEXMAN" project (ID:LI 2811/1–1) funded by DFG, National Natural Science Foundation of China under Grant (NO.62273081).

Data Availability The datasets used or analyzed during the current study are available from the corresponding author on reasonable request.

Code Availability The code during the current study is available from the corresponding author on reasonable request.

Declarations

Ethics Approval Not applicable.

Consent to Participate Not applicable.

Consent for Publication All authors agree to publish the paper.

Conflicts of Interest All authors disclosed no relevant relationships.

References

1. Landi, C.T., Ferraguti, F., Secchi C.: Tool compensation in walk-through programming for admittance-controlled robots. In Proceedings of the Annual Conference of IEEE Industrial Electronics Society, Firenze, Italy, 2016.
2. Ferraguti, F., Landi, C.T., Sabattini, L.: A variable admittance control strategy for stable physical human-robot interaction. Int J Rob Res **38**(6), 747–765 (2019)
3. Li, Q., Schürmann, C., Haschke, R., Ritter, H.: A control framework for tactile servoing. Proceedings of Robotics: Science and Systems, Berlin (2013). https://doi.org/10.15607/RSS.2013.IX.045
4. Albu-Schäffer, A., Haddadin, S., Ott, C., Stemmer, A., Wimböck, T., Hirzinger, G.: The DLR lightweight robot: design and control concepts for robots in human environments. Ind Rob: Int J **34**(5), 376–385 (2007)
5. Haddadin, S., Luca, A.D., Albu-Schaffer, A.: Robot collisions: a survey on detection, isolation, and identification. IEEE Trans Robot **33**(6), 1292–1312 (2017)
6. Wahrburg, A., Bös, J., Listmann, K.D., Dai, F., Matthias, B., Ding, H.: Motor-Current-Based Estimation of Cartesian Contact Forces and Torques for Robotic Manipulators and Its Application to Force Control. IEEE Trans Autom Sci Eng **15**(2), 879–886 (2018)
7. Liu, G., Li, Q., Fang, L., Han, B.: A new joint friction model for parameter identification and sensor-less hand guiding in industrial robots. Ind Rob: Int J Rob Res Appl **47**(6), 847–857 (2020)
8. Keemink, A.Q., Kooij, H.V.D., Stienen, A.H.A.: Admittance control for physical human-robot interaction. Int J Rob Res **37**(11), 1421–1444 (2018)
9. Ficuciello, F., Romano, A., Villani, L.: Cartesian impedance control of redundant manipulators for human-robot co-manipulation. In Proceedings of the IEEE International Conference on Robotics and Automation, Chicago, USA (2014)
10. Liu, G., Han, B.: Improving robotic impedance control performance employing a cascaded controller based on virtual dynamics model. Proc Inst Mech Eng C J Mech Eng Sci **236**(3), 1815–1825 (2022)
11. Campeau-Lecours, A., Mayer-St-Onge, B., Gosselin, C.: Variable admittance control of a four-degree-of-freedom intelligent assist device. In Proceedings of the IEEE International Conference on Robotics and Automation, Minnesota, USA (2012)
12. Burdet, E., Osu, R., Franklin, D.W., Milner, T.E., Kawato, M.: The central nervous system stabilizes unstable dynamics by learning optimal impedance. Nature **414**(6862), 446–449 (2001)
13. Yang, C., Ganesh, G., Haddadin, S., Parusel, S., Albu-Schaeffer, A., Burdet, E.: Human-like adaptation of force and impedance in stable and unstable interactions. IEEE Trans Rob **27**(5), 918–930 (2011)
14. Naceri, A., Schumacher, T., Li, Q., Calinon, S., Ritter, H.J.: Learning optimal impedance control during 3D arm movements. IEEE Robot Autom Lett **6**(2), 1248–1255 (2021)
15. Lawrence, D.A., Marietta, M.: Impedance control stability properties in common implementations. In Proceedings of the IEEE International Conference on Robotics and Automation, Denver, USA (1988)
16. Tsumugiwa, T., Yokogawa, R., Yoshida, K.: Stability analysis for impedance control of robot for human-robot cooperative task system, vol. 4, pp 3883–3888. 2004 IEEE/RSJ International Conference on Intelligent Robots and Systems (IROS) (IEEE Cat. No.04CH37566), Sendai (2004). https://doi.org/10.1109/IROS.2004.1390020
17. Kronander, K., Billard, A.: Stability considerations for variable impedance control. IEEE Trans Rob **32**(5), 1298–1305 (2016)
18. Peer, A., Buss, M.: Robust stability analysis of bilateral teleoperation systems using admittance-type devices. In SICE Annual Conference, Tokyo, Japan (2008)
19. Tsumugiwa, T., Yokogawa, R., Hara, K.: Variable impedance control based on estimation of human arm stiffness for human-robot cooperative calligraphic task. In Proceedings of the IEEE International Conference on Robotics and Automation (2002)
20. Wang, Z., Angelika, P., Martin, B.: Fast online Impedance Estimation for Robot Control. Proceedings of the 2009 IEEE International Conference on Mechatronics. Malaga, Spain, pp. 978–983 (2009)
21. Duchaine, V., Gosselin, C.M.: Investigation of human-robot interaction stability using lyapunov theory. In Proceedings of the IEEE International Conference on Robotics and Automation, Pasadena, USA (2008)
22. Ranatunga, I., Cremer, S., Popa, D.O., Lewis, F.L.: Intent aware adaptive adimttance control for physical human-robot interaction. In Proceedings of the IEEE International Conference on Robotics and Automation (2015)
23. Kang, G., Oh, H.S., Seo, J.K., Kim, U., Choi, H.R.: Variable admittance control of robot manipulators based on human intention. IEEE/ASME Trans Mechatron **24**(3), 1023–1032 (2020)
24. Li, Y., Ge, S.: Human-robot collaboration based on motion intention estimation. IEEE/ASME Trans. Mechatronics **19**(3), 1007–1014 (2014)
25. Ryu, D., Song, J.B., Choi, J.: Frequency domain stability observer and active damping control for stable haptic interaction. In Proceedings of the IEEE/RSJ International Conference on Intelligent Robots and Systems, pp. 3611–3616 (2007)
26. Dimeas, F., Aspragathos, N.: Online stability in human-robot cooperation with admittance control. IEEE Trans Haptics **9**, 267–278 (2016)
27. Cook, C.S., McDonagh, M.J.N.: Measurement of muscle and tendon stiffness in man. Eur J Appl Physiol **72**(4), 380–382 (1996)

Guanghui Liu received the M.E. degree in control theory and control engineering from the College of Information Science and Engineering, Northeastern University, Shenyang, China, in 2018. He is currently working toward the Ph.D. degree in Robotic Science and Engineering from the Faculty of Robot Science and Engineering, Northeastern University, Shenyan, China. His research interests include model identification, physical human-robot interaction, and path planning.

Qiang Li received Ph.D. degree in pattern recognition and intelligence systems from the Shenyang Institute of Automation (SIA), Chinese Academy of Sciences (CAS), Shenyang, China, in 2010. He was awarded stipend from the Honda ResearchInstitute Europe, Offenbach, Germany. From 2009 to 2012, he started his postdoctoral researching with theCoR-Lab, Bielefeld University, Bielefeld, Germany. Currently, he is currently a Project Investigator of DEXMAN sponsored by the Deutsche Forschungsgemeinschaft (DFG), Bonn, Germany, and is working with Neuroinformatics Group, Bielefeld University. His current research interests include tactile servoing and recognition, sensory-based robotic dexterousmanipulation, and robotic calibration and dynamic control.

Lijin Fang received B.E. degree in Electrical automation from Xian Jiaotong University, Xian, China, in 1988. He was funded by the Chinese government to study in Russia in1992 and received the Ph.D. degree in 1996. He is currently a Professor with the Faculty of Robot Science and Engineering, Northeastern University, Shenyang, China. His research interests include dynamics based robot precision control, robot imitating muscle drive and intelligent control, research and design of climbing mobile robot.

Hualiang Zhang received B.E. degree in measurement and control technology and instruments from the Huazhong University of Science and Technology, Wuhan, China, in 1998. He received Ph.D. degree in Mechatronic Engineering from the Shenyang Institute of Automation (SIA), Chinese Academy of Sciences (CAS), Shenyang, China, in 2010. He is currently an associate research fellow with the Key Laboratory of Industrial Control Network and System, Shenyang Institute of Automation, Chinese Academy of Sciences, Shenyang, China. His research interests include intelligent robot operating system, motion controller hardware-in-the-loop simulation.